Sensors and Actuators A 236 (2015) 394–404

Contents lists available at ScienceDirect

Sensors and Actuators A: Physical

journal homepage: www.elsevier.com/locate/sna

Micro-tweezers: Design, fabrication, simulation and testing of a pneumatically actuated micro-gripper for micromanipulation and microtactile sensing☆

A.F. Alogla, F. Amalou, C. Balmer, P. Scanlan, W. Shu*, R.L. Reuben

School of Engineering and Physical Sciences, Heriot-Watt University, Edinburgh, United Kingdom

ARTICLE INFO

Article history:
Received 1 November 2014
Received in revised form 25 June 2015
Accepted 25 June 2015
Available online 20 July 2015

Keywords:
Micro-gripper
Pneumatic
Micromanipulation
Finite element analysis
Tactile sensing

ABSTRACT

This paper presents a novel micro-gripper design with the dual functions of manipulation and force sensing. The device consists of two parallel plates, each mounted on torsion bars, which can be made to rotate towards or away from each other by use of a pneumatically- or hydraulically-actuated elastic membrane. The plates can be conveniently fabricated using photo-etching and the design allows for a range of ratios between actuation pressure and tip opening displacement and force. The elastic gripping tips can be designed to provide sufficient compliance that their strain can be used to monitor and control the gripping force. An exemplar device has been fabricated and its behaviour characterised by a series of mechanical measurements of force and displacement. These measurements have been rationalised using a simple analytical model, backed up with finite element analysis to emphasise the design variables and scalability. This exemplar device, with a maximum tip opening amplitude of 1 mm and maximum force output of 50 mN, has also been demonstrated to perform pick-and-place operations with 200 μm micro-beads.

1. Introduction

The rapid evolution in the biological sciences has led to an increased requirement for manipulating entities at the micro- and nano-scale. In general, manipulating biological objects such as single cells, micro-beads or even embryos can be classified into contact and non-contact techniques. The non-contact techniques are mainly optically-based [1–4], where a highly focused laser beam is used to trap and move a biological micro-object. Although the performance of such techniques is satisfactory, sophisticated and expensive optical setups are required [5] and the exposure to optical radiation may have long term negative effects on the manipulated micro-objects [6].

Micro-pipettes and grippers are the most commonly used contact techniques for manipulating biological micro-objects. Pipettes use a negative pressure applied through a nozzle but, despite its capability to manipulate single cells, this technique requires a highly skilled user to achieve the manipulation without damage to the cells as it is not possible to very accurately control the forces acting on the object being manipulated. Furthermore, pipettes have limited versatility and, if cells are smaller than the opening of the pipette nozzle, several can be drawn into the pipette rather than isolating just one [7]. Micro-grippers show much greater versatility to manipulate a range of object sizes and also the possibility of controlling and measuring the forces acting on the gripped objects.

Micro-grippers are complex micro-electro-mechanical-systems (MEMS) [8] and can be categorized according to their actuation mechanism: electrostatic, shape memory alloy (SMA), magnetic or piezoelectric, each of which has its advantages and disadvantages. Electrostatic actuation generates a satisfactory amount of output force [9] but is difficult to operate in ion-rich liquids (e.g. body fluids [10]). SMA actuators, while producing a high force and displacement, are problematic in liquid environments due to the heat loss associated with the high surface-to-volume ratio of microdevices which may damage the biological surroundings [10]. Furthermore, the displacements of SMAs are hard to control because of their thermomechanical nonlinearities [11]. Piezoelectric actuation offers high speed and good motion resolution [12] but actuation displacements are limited [13] and the required applied voltages can damage biological systems. Due to the disadvantageous scaling of magnetic fields, magnetic microactuators have low force output and their performance is also limited because of thermal dissipation by the conductive materials and the possibility of significant

☆ Selected papers presented at EUROSENSORS 2014, the XXVIII edition of the conference series, Brescia, Italy, September 7–10, 2014.

* Corresponding author. Tel.: +44 1314518165.
E-mail address: w.shu@hw.ac.uk (W. Shu).

http://dx.doi.org/10.1016/j.sna.2015.06.032

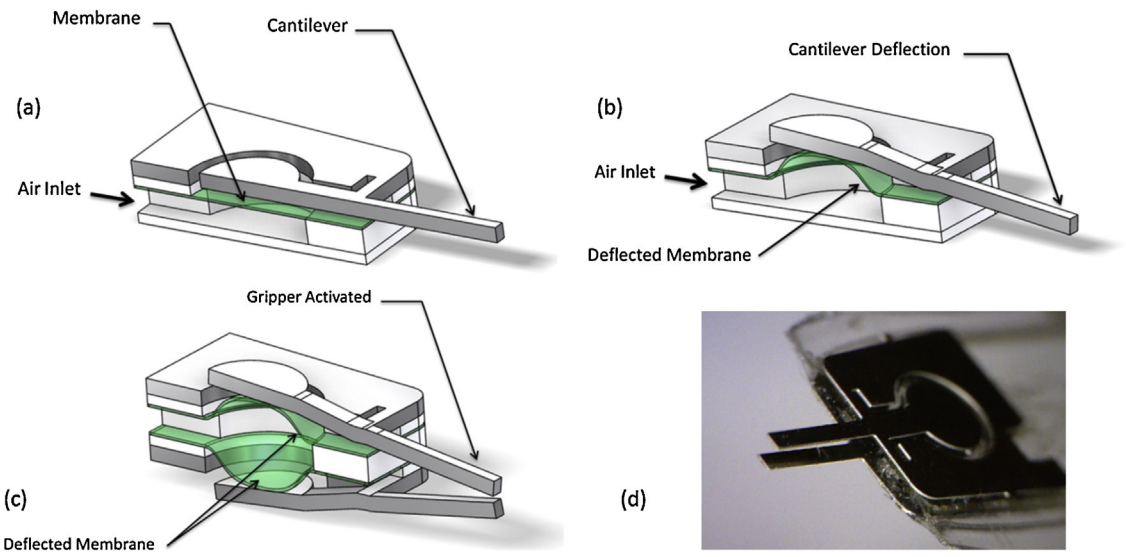

Fig. 1. Schematic drawings of working principle of the gripper device (a–c), and picture of assembled micro-gripper (d).

electrical leakage currents. Also, magnetic fields can pose problems in the biological environments [14].

Fluidic microactuators, with their high force and power densities, have been widely advocated for manipulating precise amounts of liquid within microfluidic and micro total analysis systems (μTAS) [15,16]. The actuation can be either pneumatic or hydraulic, and can therefore operate in liquid environments for biological cell manipulation [17–19]. Although there are relatively few studies of this type of actuator it has been demonstrated that pneumatic actuators have the potential to produce some of the highest force and power densities of actuation options at the microscale [15]. High performance pneumatic micro-gripper can be fabricated using micro-stereolithography [20] or laser cutting [21]. Despite the advantages of this type of actuator, designs typically require complex 3-dimensional fabrication or 3-dimensional assembly techniques and hence limited the possibility for large-scale production. This paper reports the design of a micro-gripper with a simple method of manufacture and assembly that has the potential to scale to the level of manipulating a single biological cell. The main design challenge is to achieve accurate control over the opening and closing states of the gripper, along with the gripping forces, which has been addressed by a compliant gripper design offering the opportunity for force feedback and two-way actuation allowing opening and closing actions.

1.1. Micro-gripper design and fabrication

The micro-gripper described here is pneumatically actuated and is designed to be operated in a range of environments, including air and liquid, at a range of scales. It comprises two main parts; the actuation mechanism and the flexible gripper arms (Fig. 1a and b). The actuator is essentially a flexible membrane that applies force to the gripper pad when the air inlet is pressurised. The gripper plate was cut from stainless steel sheet (50 μm in thickness, Goodfellow UK Ltd) using a photo-etching technology to give an outer envelope, which was sandwiched between two PMMA (poly methyl methacrylate) layers. When pressure is applied to the pad, the arms pivot around a torsional spring consisting of a bar-shaped ligament of the gripper plate. The arms themselves are designed to be flexible so that the gripping force can, in principle, be monitored by measuring the strain at the pivot end of the arm or the slope at its free end. The design can be operated with two arms closing together when actuated (as shown in Fig. 1c) or with one arm bearing onto either a fixed plate or a sample surface (as shown in Fig. 1c). It can also be actuated in the reverse direction so that the jaws are opened by actuators on the opposite sides of the gripper plates using the spring force and compliance of the arms to offer the gripping force, limited, if necessary, by the air pressure. The whole design is scalable by controlling the dimensions of the components of the gripper, in particular the arms and torsion bars.

This micro-gripper is assembled with multilayers (in Fig. 2) of thin PMMA sheet (200 μm in thickness, EMKAY Plastics Ltd), elastic silicone membrane (50 μm in thickness) and double-sided adhesive sheet (50 μm, 3 M UK Plc), which are fabricated using a CO_2 laser system [22]. This device is assembled by coating the PMMA with double sided adhesive and then laser cutting the layers. These layers are then manipulated by tweezers into the correct position. The whole device is then covered in laminate film and heated to ensure no chance of leaks. The assembly of this device is a simple and cost effective method of manufacture of a micro-gripper, the use of layers also lends itself to large scale production, Fig. 3, and additional layers can offer further actuation options, such as channels for gripper closing.

2. Performance of prototype device

To validate the above-mentioned design principles, a prototype device was realised in 50 μm thick stainless steel sheet with a pad diameter of 2 mm, arms of length 3 mm and breadth 0.45 mm, and torsion bars of breadth 0.3 mm and length 0.625 mm. The performance of the device was evaluated using two tests; a dynamic test where the feed air pressure was pulsed at a range of frequencies and pressures and the tip displacement with no loading was measured, and a static test where the input pressure and output load were measured.

For the dynamic test, an optical sensor was used to obtain the deflection at the cantilever tip using a similar approach to an AFM where a laser beam at a fixed angle is reflected from the end of the cantilever and the position of the spot on a photodetector recorded, Fig. 4(a). The deflection was calculated from the voltage of the laser using the geometry of the experimental setup [24]. Deflection data were acquired using a LabView control interface at a rate of 300 samples per second for a record length of around 20 cycles (e.g. Fig. 4(b)) whilst the pressure was pulsed from zero to 1, 2, 3, 4, and 5 bar at frequencies of 1, 2, 4, 8, 20, 50, 100, and 300 Hz. However,

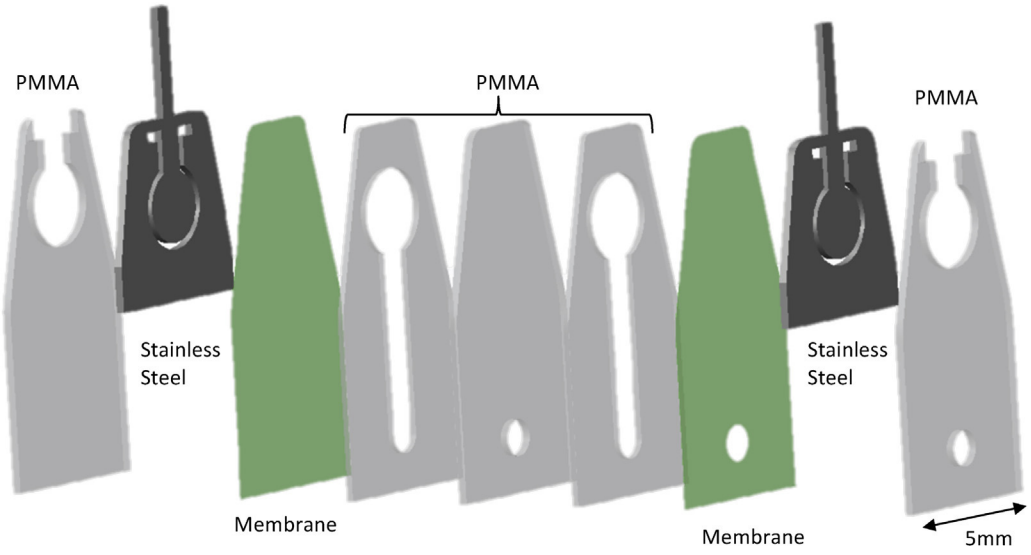

Fig. 2. Assembly steps.

the elasticity of the pressure feed dampens te pressure oscillation and frequencies above 50 Hz are of little meaning.

The relation between the deflection of the micro-gripper pad and micro-gripper tip is an important design consideration since it informs the torsional stiffness of the pivot bars as well as the tip sensitivity to gripping force. This relation was measured using a modification of the dynamic set-up shown in Fig. 4(a), where the deflection of the pad and the tip were measured in separate experiments for pressure pulses to 0.17, 0.35, 0.56 and 0.76 bar, all at a frequency of 1 Hz. Fig. 5 shows the mean and standard deviation of the amplitudes of tip displacement and pad displacement for each of the pressures plotted against each other.

For the static tests, a digital balance with read-out up to four decimal places (in grammes) was used to measure the force generated at the tip of the cantilever. The tip was brought into contact with a 1.5 mm diameter metallic ball mounted on a lightweight conical holder as shown schematically in Fig. 6(a).

The pressure in the feed line was then increased incrementally to 5 bar, recording the output force at approximately 0.2, 0.3, 0.4, 0.5 and 1 bar, and thereafter at 1 bar intervals. The results are shown in Fig. 6(b) for forward and reverse increments of pressure up to 5 bar using two dwell times (10 s and 30 s) before the force was recorded. The same procedure was used to determine the input force for a given pressure by applying the membrane directly to the metal ball and recording the force at the same increments of pressure. Fig. 6(c) shows the relationship between the input force as defined by the input pressure and the output force, determined from the mass exerted on the balance, for each of the pressure increments.

3. Analytical model

In order to select appropriate dimensions for a tactile gripper of the type presented, it is useful to have a simple analytical model for the stiffnesses of its key parts. Fig. 7 shows a simplified mechanical model of the gripper pad-arm plate, with the input force, the output reaction and the torsional springs (Fig. 8).

When the cantilever tip is not in contact with an object ($R_{output} = 0$), the input force determines the reaction torque:

$$T = 2.35F_{input},$$

for an input force in N and torque in N mm. For small displacements, the angular displacement at the bars can be written in terms of the dimensions of the plate:

$$\theta = \frac{TL}{KG} = 0.841F_{input}$$

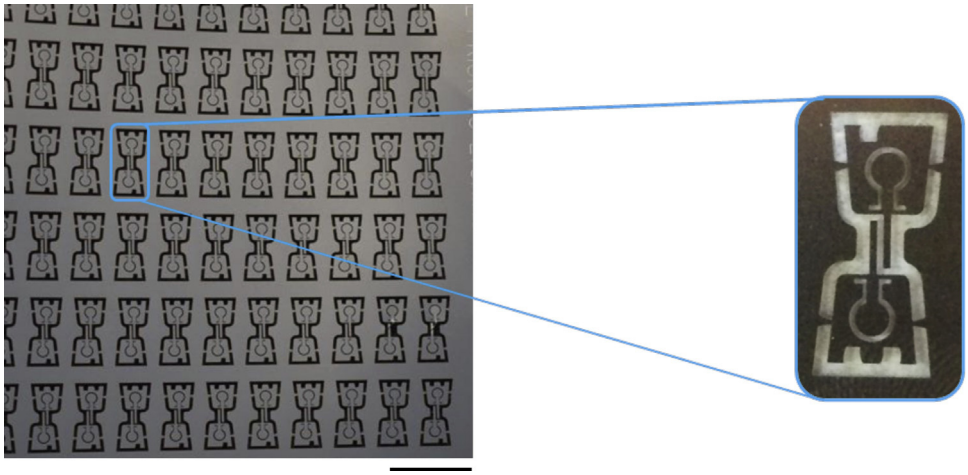

Fig. 3. Array of photo etched micro-grippers (scale bar 15 mm).

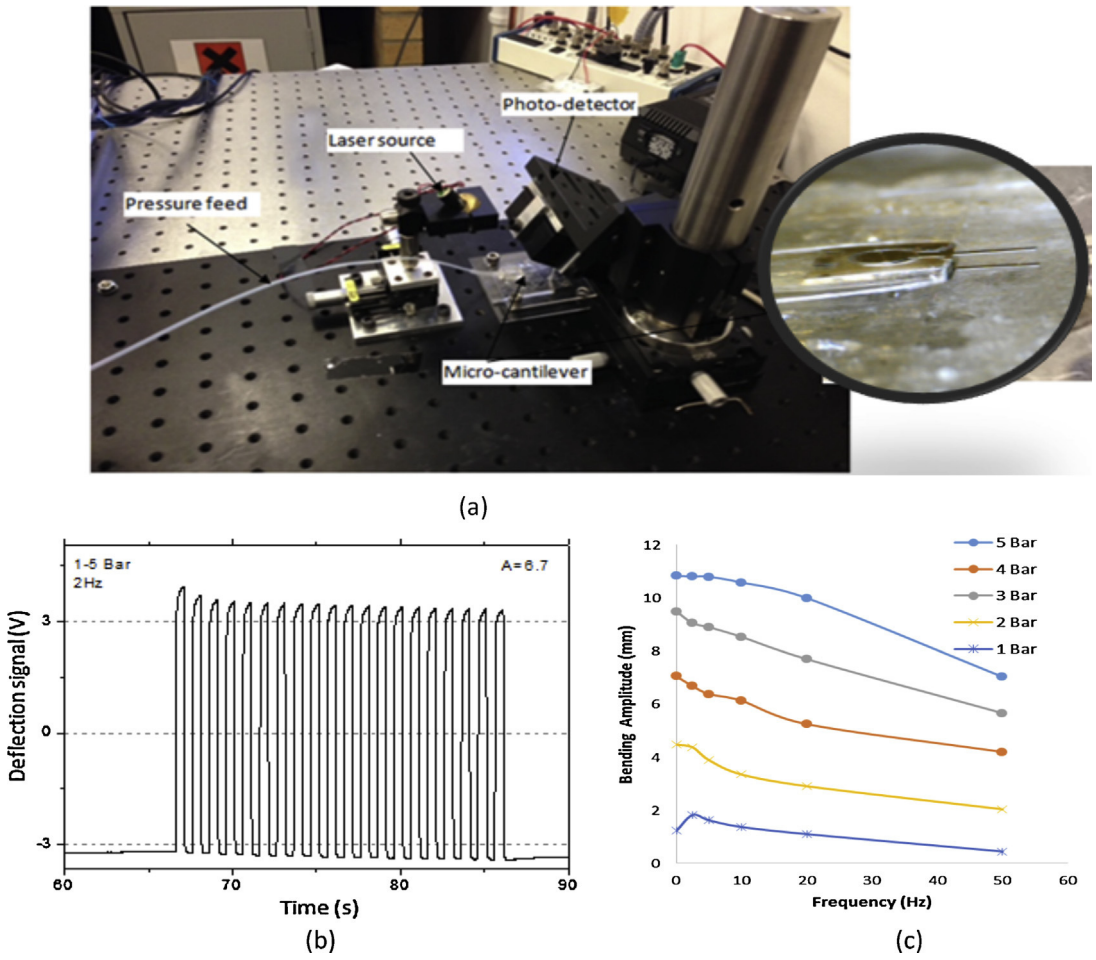

Fig. 4. (a) Dynamic test set-up with optical sensor, (b) Typical dynamic test output from optical sensor, (c) amplitude of tip displacement as frequency is varied for different pulsed pressures.

where L is the length of the cantilever, G is the shear modulus and the torsion constant of the bars:

$$K = ab^3\left[\frac{16}{3} - 3.36\frac{b}{a}\left(1 - \frac{b^4}{12a^4}\right)\right]$$

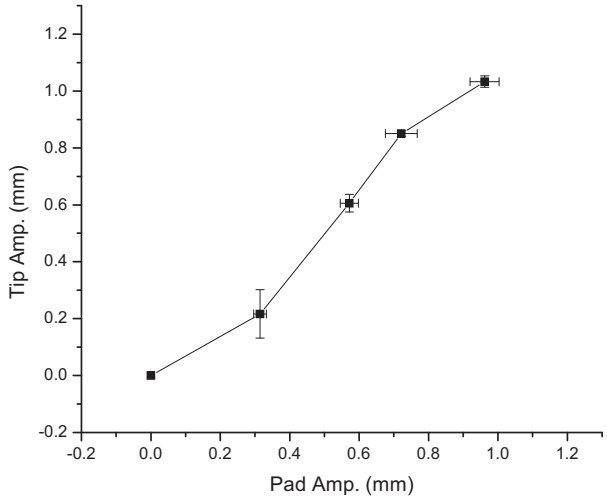

Fig. 5. Relation between measured pad and tip deflections for pressure pulse amplitudes between 0.1 and 0.75 bar.

and $2a$ and $2b$ are the short and long dimensions of the torsion bar cross-sections.

The expected tip displacement for a given angle is $\delta_{arm} = l_{arm}\tan\theta = l_{arm}\tan(0.841F_{input})$ mm and, for a simple torsion pivot (i.e. no bending), the displacements at the pad and at the cantilever tip for a given angle (i.e. a given pressure) might therefore be expected to be related $\delta_{cantilever,T} = \frac{l_{cantilever}}{l_{pad}}\delta_{pad,T}$

As well as causing the above displacements, an input force might be expected to introduce certain amount of bending in the pad arm, depending on the torsional spring stiffness, also bending in the cantilever arm, depending on the reaction force of the gripped object. To a first approximation, the pad itself can be assumed not to bend so that the bending component of the pad displacement can be taken as the end deflection of a cantilever of length L where the load plus an additional applied moment $M_{input} = F_{input}(L-l)$ is applied a distance l from the fixed end. The relevant displacements at the pad are given by $\delta_{pad} = \delta_{arm} + \text{slope}_{arm}(L-l)$, so:

$$\delta_{pad,b} = \frac{1}{0.841}\tan^{-1}\left(\frac{\delta_{cantilever,T}}{3.15}\right)\frac{1}{EI}\left[\frac{l^3}{3} + l^2\left(l_{pad} - l\right) + l\left(l_{pad} - l\right)^2\right]$$

$$= \frac{1}{0.841}\tan^{-1}\left(\frac{\delta_{cantilever,T}}{3.15}\right)\frac{12}{193\times10^3\times0.75\times0.05^3}$$

$$\left[\frac{1.2^3}{3} + 1.2^2(2.2-1.2) + 1.2\times(2.2-1.2)^2\right]$$

$$= 0.789\tan^{-1}\left(\frac{\delta_{cantilever,T}}{3.15}\right)[3.22] = 2.536\tan^{-1}\left(\frac{\delta_{cantilever,T}}{3.15}\right)$$

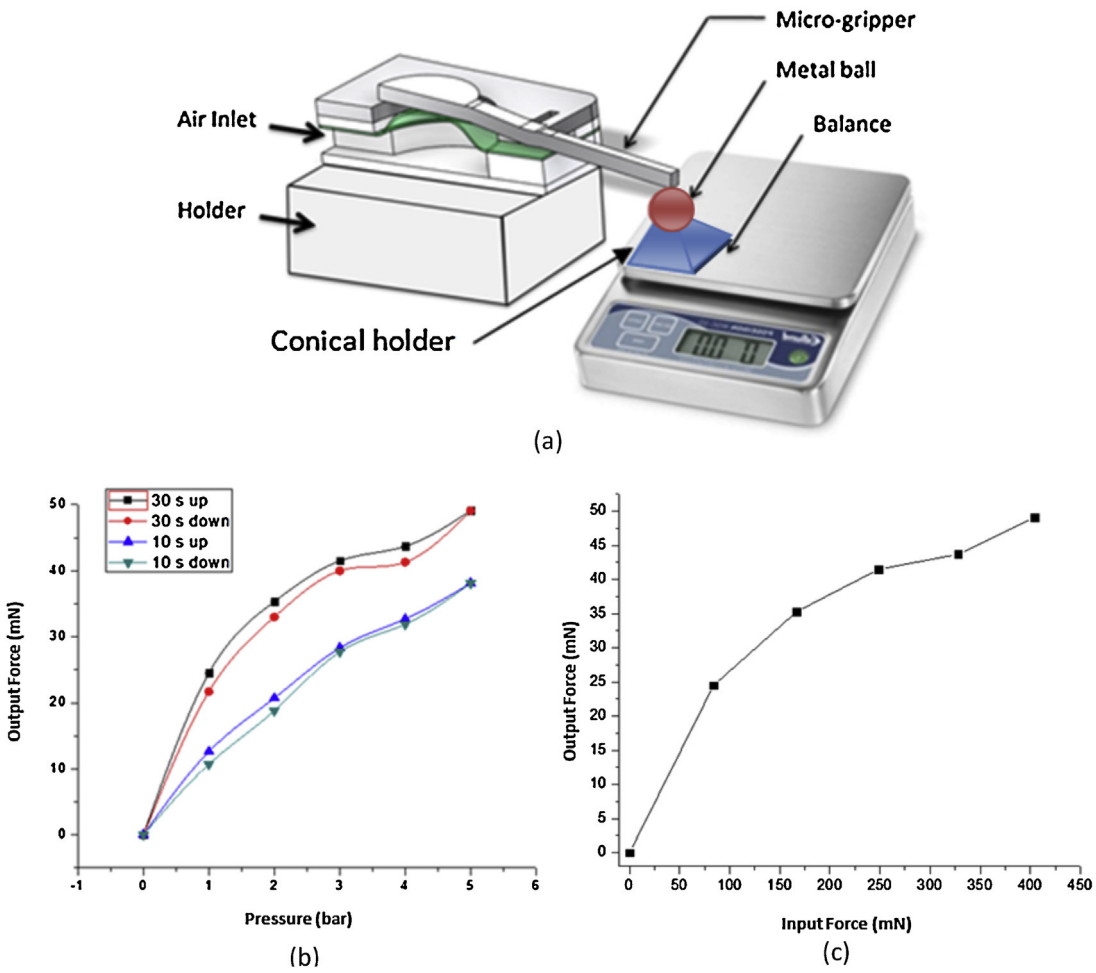

Fig. 6. (a) Schematic test set-up for static loading of cantilever), (b) Measured cantilever tip (output) force vs. input pressure, (c) Measured input and output forces at pressures used in (b) with 30 s dwell time.

Thus, the relationship between pad displacement and tip displacement for an unloaded tip can be expressed as:

$$\delta_{\text{pad}} = 0.746\delta_{\text{cantilever}} + 2.536\tan^{-1}\left(\frac{\delta_{\text{cantilever}}}{3.15}\right) \quad (1)$$

Fig. 10 shows the mean data from Fig. 6 for measured pad and tip displacements for the four increments of pressure. Also, for each of the tip displacements, the corresponding pad displacements have been calculated, first assuming the torsion bars to act merely as pivots (i.e. no torsional stiffness) and, second, taking into account the stiffness of the torsion bars. As can be seen, the second calculation is reasonably consistent with the measurements indicating that the analytical model is sufficient for the purposes of sizing the torsion bars. A finite element model of the plate including the outer frame was also built and this was loaded using the membrane pressure

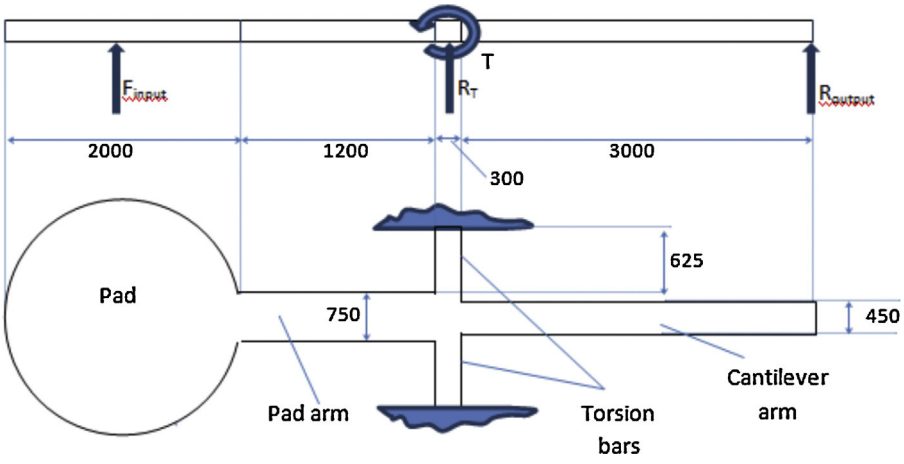

Fig. 7. Simplified mechanical model of cantilever.

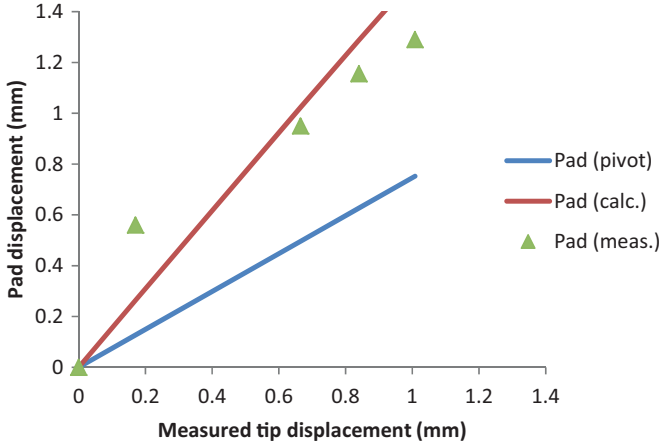

Fig. 8. Analytical model of cantilever for assessing pad displacment compared with measured values (Fig. 4).

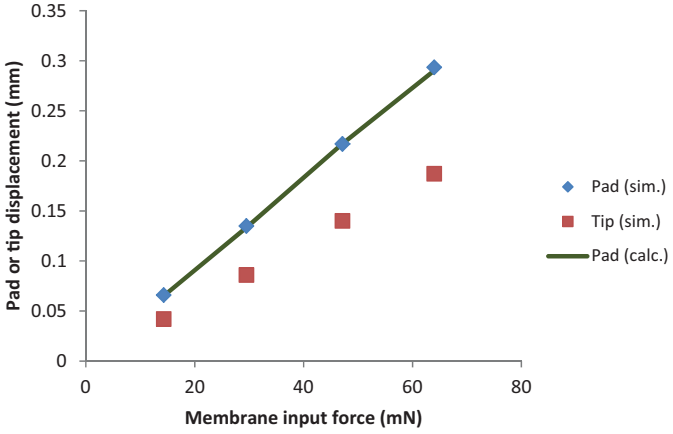

Fig. 10. Simulated pad and tip displacements for pressure loading of the pad at values shown in Fig. 4. Solid line shows calculated pad displacement (using Equation (1)) for each of the simulated tip displacements.

applied over the surface of the pad, but simulated as a point force at the centre of the pad (Fig. 9). Fig. 10 shows the resulting pad and tip displacements for each of the pressures used in the static tests, alongside calculated values of the pad displacement for each of the simulated tip displacements using Equation (1), showing that, at this limited range of input pressures the elastic simulation and the elastic analytical model are in agreement.

Based on this tentative verification, the analytical model can now be used to assess the input force corresponding to the various pressure amplitudes seen in Fig. 4(c). However, Fig. 4(c) shows that the maximum tip displacement for the unloaded cantilever depends on actuation frequency at least up to 50 Hz above which the actuator is probably limited by the supply of air. The frequency sensitivity is unlikely to be due to a structural resonance (for example, the natural frequency of the least stiff part of the system, the cantilever, is about 4 kHz) nor is it likely, given the data in Fig. 6(a), to be due to membrane relaxation or leakage. Figs. 11 and 12 show the variation of maximum tip displacement (as voltage output from the photodetector) with input pressure pulse height at the actuator (data essentially re-plotted from Fig. 4(b)). The curves are reasonably linear (more so at lower frequencies) and thus an overall compliance (in mm tip deflection per bar) can be determined for the actuator. This is plotted in Fig. 12 for the whole range of frequency examined, and it can be seen that the compliance changes with frequency over the range 0–50 Hz, and little thereafter. This suggests that the dynamic behaviour of the actuator is affecting the tip displacement and so the most reliable measurement of the system compliance is given by extrapolation to zero frequency (Fig. 12), i.e. a value of 0.223 mm/bar. Since this is only around 1% different to the value measured using a frequency of 1 Hz, the pad and tip measurements shown in Fig. 5 are unlikely to have been much affected by the actuator dynamic response.

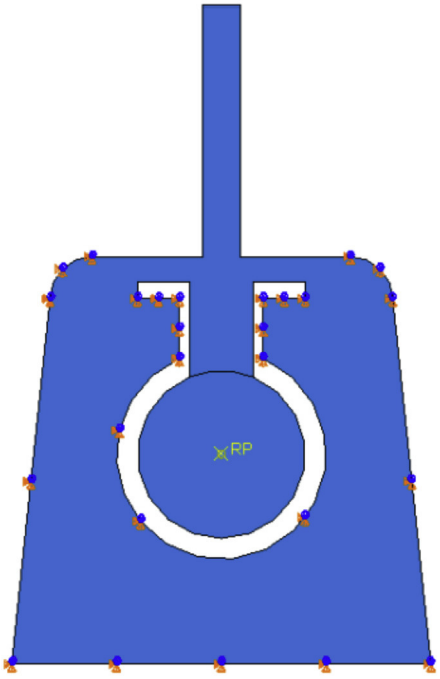

Fig. 9. FE model of gripper plate for assessing pad and tip displacments for a force applied at RP.

The compliance can further be used to determine the input force corresponding to a given input pressure when the output force, $R_{output} = 0$ using the relationship between input force and cantilever displacement:

$$F_{input, R_{output}=0} = \frac{1}{0.841} \tan^{-1}\left(\frac{0.223p}{3.15}\right) \quad (2)$$

where the input pressure, p, is in bar. When the cantilever is loaded, the force system becomes statically indeterminate which makes an analytical model a bit more tedious and so, for the purposes of this paper, the analytical relationship between the input pressure and input force (Equation (2)) was used in a linear elastic FE simulation of the gripper plate with a loaded cantilever to calculate the output force. The results of this simulation are compared with the measured output forces at 30 s dwell time from the static tests (Fig. 6(b)), and it can be seen that agreement is good up to a pressure of 1 bar, beyond which the simulated output force is higher than that measured, the discrepancy increasing with increasing pressure. The reason for this can be seen in the finite element elastic stress distribution calculated at 1 bar input pressure shown in Fig. 13. Notwithstanding the local stresses, it can be seen that the von Mises stress at the torsion bar end on the input pad arm is about 800 MPa, whereas that at the fixed ends of the torsion bars is about 500 MPa, both values prevailing across most of the relevant cross-section. These stresses are beyond the yield stress of moderately cold-worked stainless steel and well beyond yield for annealed stainless steel [23], so it is likely that the reduction in experimental force output is due to the formation of one or more plastic hinge in the gripper plate. Plastic collapse would invalidate the relationship between input force and pressure (Equation (2)) so

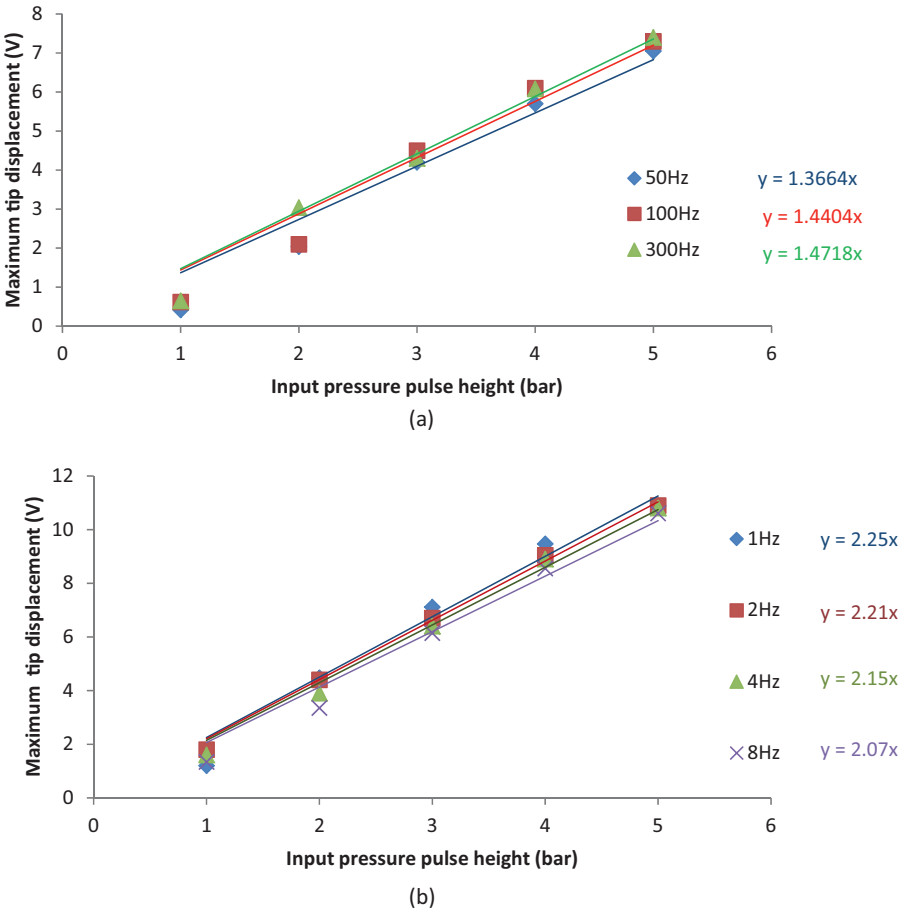

Fig. 11. (a) Effect of frequency on unloaded cantilever system compliance at higher frequencies (data from Fig. 4), (b) effect of frequency on unloaded cantilever system compliance at lower frequencies (data from Fig. 4).

that the simulation would be in error in terms of the input as well as in terms of the resulting deflections. At any rate, Equations (1) and (2) can still be used for design purposes so that dimensions of the gripper can be chosen to avoid yield using very simple analytical expressions (Fig. 14).

The next step for this work is further development of the tactile sensing of micro-objects. Extending the considerations above, and assuming no bending, the static stiffness of a gripped linear elastic object, k, can be obtained (for conceptual design purposes) by considering the relationship between the angular displacements θ_1 and θ_2 with and without, respectively, the object in place:

Without the object:

$$l_1 \cos\theta_1 \times F_{\text{in}} = \frac{\theta_1 JG}{L}$$

With the object gripped:

$$l_1 \cos\theta_2 \times F_{\text{in}} = \frac{\theta_2 JG}{L} + l_2 \cos\theta_2 \times k\delta_{\text{obj}}$$

So

$$F_{\text{in}} l_1 = \frac{\theta_1 JG}{L\cos\theta_1} = \frac{\theta_2 JG}{L\cos\theta_2} + l_2 k\delta_{\text{obj}}$$

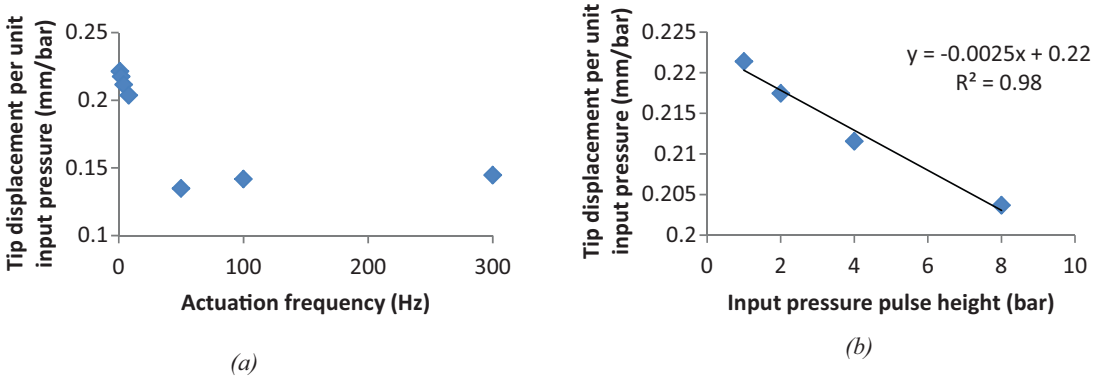

Fig. 12. (a) Unloaded system compliance over full frequency range, (b) unloaded system compliance at low frequencies.

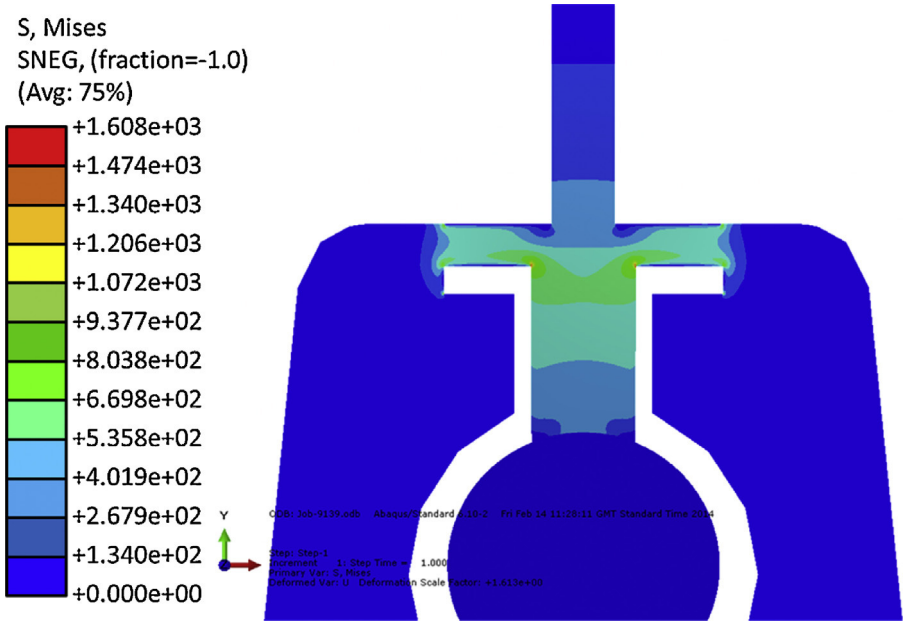

Fig. 13. Elastic stress analysis for loaded gripper plate with applied pressure of 1 bar.

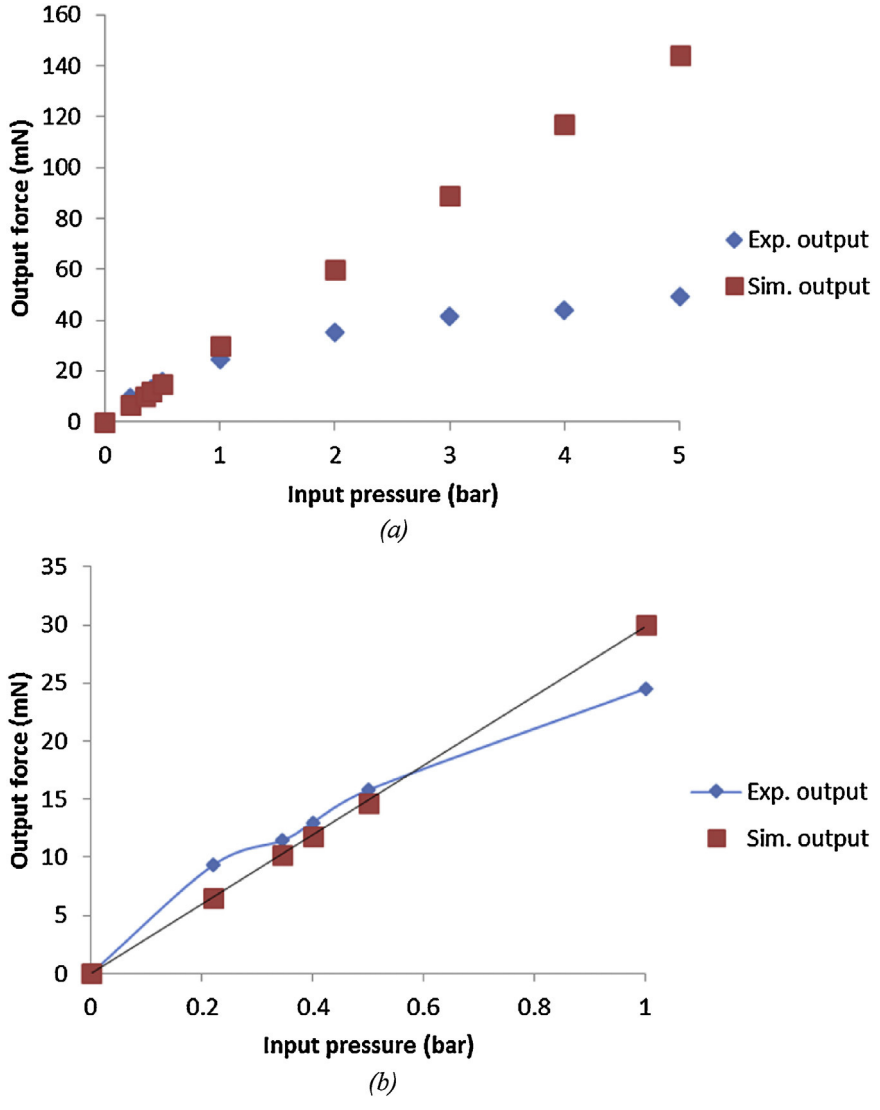

Fig. 14. Measured and simulated aoutput forces for a range of input pressues (a) range from 0 to 5 bar, (b) range from 0 to 1 bar.

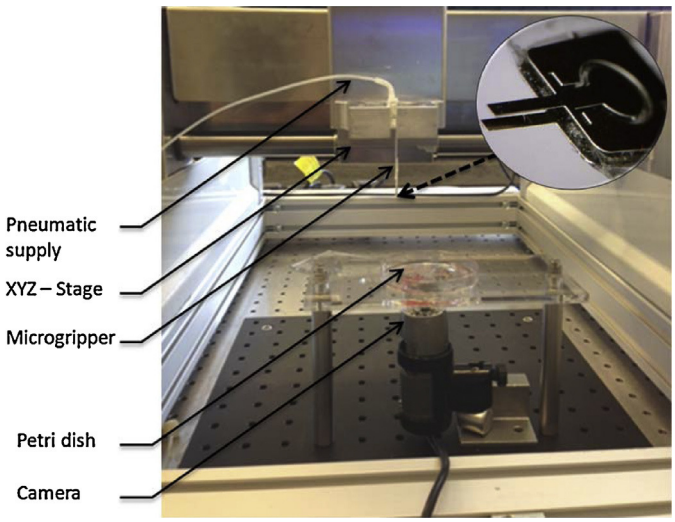

Fig. 15. Experimental seutp for pick-and-place demonstration.

or

$$k = \frac{JG}{L\delta_{obj}l_2}\left(\frac{\theta_1}{\cos\theta_1} - \frac{\theta_2}{\cos\theta_2}\right) \quad (3)$$

where l is the perpendicular distance between the cantilever tip and torsion springs and L is the total length of the torsion springs. Acknowledging the assumptions of its derivation, Equation (3) could be used to measure the static stiffness of a gripped object provided that the amount of its compression (δ_{obj}) can be measured and that the angles θ_1 and θ_2 can be measured. Equally the stiffness of a viscoelastic object could be assessed by recording the amplitude of the cantilever tip whilst grasping an object at different frequencies.

Once the technique has been validated with gripped elastic and viscoelastic objects using similar measurements to these reported here, the next stage is to develop a generic design approach which allows the necessary measurements to be made at the input side of the gripper where intervention is easier in real applications.

4. Device demonstration

A fully-assembled version of the device was used to demonstrate the actuator in pick-and-place mode, in air and underwater. The demonstration consisted of manipulating acid washed zirconium micro-beads of 200 μm diameter (OPS Diagnostics, Lebanon NJ, USA), for which the exemplar device reported above was mounted on an XYZ stage and the micro-beads placed in a petri-dish with a monitoring camera underneath, as shown in Fig. 15.

The above-mentioned arrangement demonstrated a very satisfactory performance both in air and under water. Fig. 16 shows the precision of placement that could be achieved using the proposed manipulation technique, where 200 μm zirconium micro-beads can be precisely positioned to form either a dotted array (on the left) or a shape of a smiley face (on the right).

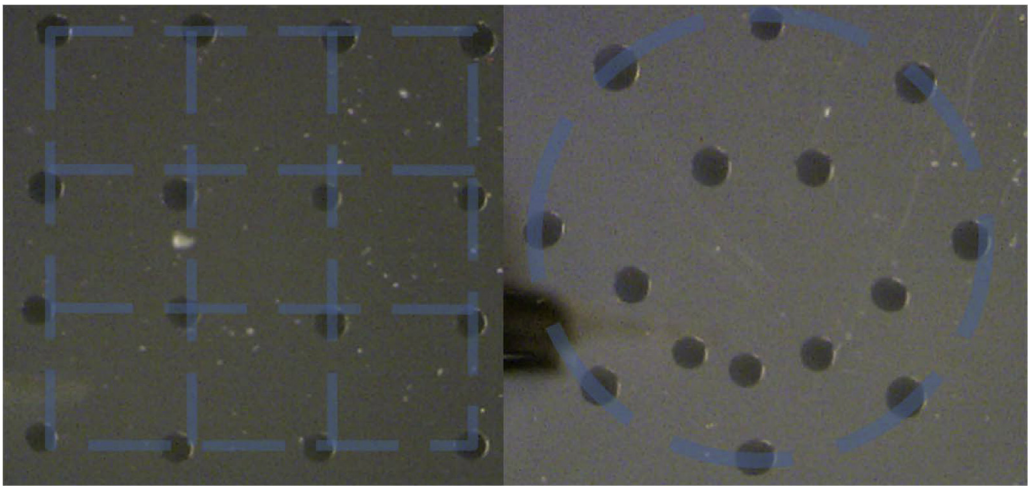

Fig. 16. Various pick-and-place arrangements of 200 μm zirconium micro-beads that are achievable with this design.

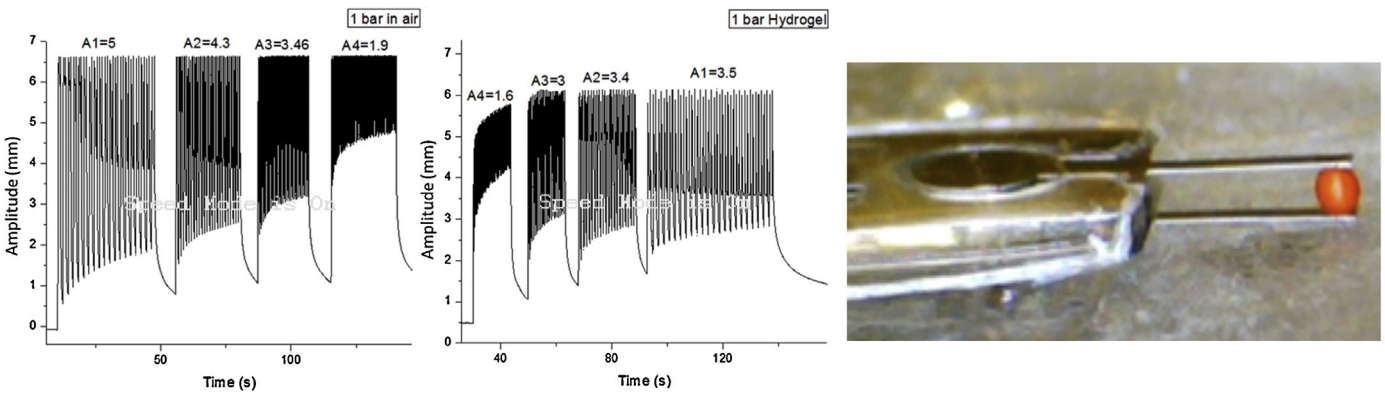

Fig. 17. Amplitude of tip under dynamic actuation, (left) free, (centre) holding a hydrogel bead and gripper holding a hydrogel bead (right).

One way in which the stiffness of gripped micro-objects can be assessed is to vibrate the cantilever at various frequencies and record the amplitude of the deflection of the cantilever. If this is done for the gripper in air and subsequently with the object gripped, the quotient of these deflections determines the stiffness of the object:

$$AR = \frac{A_{obj}}{A_{air}} \quad (4)$$

This procedure was carried out with a 1 bar actuator pressure, gripping 400 μm hydrogel beads and using frequencies of 1 Hz (A1), 2 Hz (A2), 4 Hz (A3) and 10 Hz (A4). The results, shown in Fig. 17 clearly indicate that there is a reduction in tip amplitude for the gripped bead at each frequency. The results further show that the amplitude change is different at each frequency and, furthermore, that there are changes in amplitude with time at a given frequency. This is probably due to a combination of dynamic effects within the actuator-membrane system, as well as in the response of the hydrogel bead. These matters are not pursued in the current paper, but will inform future work using devices of this type.

5. Conclusions

This work demonstrates a pneumatically actuated micro-gripper that has the ability to pick and place micron-sized objects with the potential to provide tactile feedback. The pneumatic micro-actuator can have its pressure-force relationship measured and controlled in both static and dynamic modes with a simple set up. The two stainless steel gripper arms can be fabricated using low-cost, scalable photo-etching manufacturing technique with a range of dimensions, allowing this design to be scaled to fit the chosen application. As the photo-etching manufacturing is a photo-lithography technique with high precision, it is possible to fabricate stainless steel based gripper with dimensions smaller than 100 μm for single cell manipulation. The stiffness of the two torsion bars can aid in tailoring the use of the gripper with the bars behaving almost as a pivot or used to down-regulate the input force (for more delicate tasks). Besides controlling the input and output forces, the design of the gripper arms can be tuned in order to provide a deflection of the arms, whose measurement can be used to measure the gripping force in operation and can potentially be fed back to control the force or used to assess the gripped object. Besides the potential use of gripper for manipulating embryos for cloning applications, the mechanical micro-tweezers may provide a new way to pick-and-place cell aggregates for biofabricating synthetic tissues [25,26]. Future work will focus on further miniaturization of the gripper for manipulating smaller objects (e.g. single cells) and treatment of the gripper surface to overcome potential striction issues. Further improvement of the gripper's tactile sensing may also lead to mechanical assessment of biological tissues *in vivo*.

Acknowledgements

This research work is supported by the Engineering and Physical Sciences Research Council (EPSRC) (Grant Code: EP/I019472/1). A. Alogla is grateful to the Saudi Government for a PhD scholarship. C. Balmer and P. Scanlan are grateful to EPSRC for PhD scholarship funding.

References

[1] M.L. Juan, M. Righini, R. Quidant, Plasmon nano-optical tweezers, Nature Photon. 5 (6) (2011) 349–356.
[2] X. Wang, et al., Enhanced cell sorting and manipulation with combined optical tweezer and microfluidic chip technologies, Lab Chip 11 (21) (2011) 3656–3662.
[3] H. Zhang, K.-K. Liu, Optical tweezers for single cells, J. R. Soc. Interf. 5 (24) (2008) 671–690.
[4] A. Ashkin, et al., Observation of a single-beam gradient force optical trap for dielectric particles, Opt. Lett. 11 (5) (1986) 288–290.
[5] C. Piggee, Optical tweezers: not just for physicists anymore, Anal. Chem. 81 (1) (2008) 16–19.
[6] K. König, et al., Cell damage in near-infrared multimode optical traps as a result of multiphoton absorption, Opt. Lett. 21 (14) (1996) 1090–1092.
[7] H.-Y. Chan, W.J. Li. A thermally actuated polymer micro robotic gripper for manipulation of biological cells. Proceedings ICRA'03, IEEE International Conference on Robotics and Automation, Taipei, Taiwan, 1, pp. 288–293.
[8] M. Zeman, G. Knopf, Design, kinematic modeling and performance testing of an electro-thermally driven microgripper for micromanipulation applications, J. Micromech. Microeng. 16 (2006) 1540–1549.
[9] S.A. Bazaz, F. Khan, R.I. Shakoor, Design, simulation and testing of electrostatic SOI MUMPs based microgripper integrated with capacitive contact sensor, Sens. Actuators A: Phys. 167 (1) (2011) 44–53.
[10] J. Ok, Y.W. Lu, C.J. Kim, Pneumatically driven microcage for microbe manipulation in a biological liquid environment, J. Microelectromech. Syst. 15 (6) (2006) 1499–1505.
[11] R. Velazquez, et al., A low-cost highly-portable tactile display based on shape memory alloy micro-actuators, in: Proceedings VECIMS IEEE International Conference on Virtual Environments, Human-Computer Interfaces and Measurement Systems, Gradini Naxos, Italy, 2005, pp. 121–126.
[12] J. Agnus, N. Chaillet, Overview of microgrippers and design of a micro-manipulation station based on a MMOC microgripper, in: Proceedings Computational Intelligence in Robotics and Automation, Finland, 2005, pp. 117–123.
[13] A. Menciassi, et al. A workstation for manipulation of micro objects. Proceedings ICAR'97, 8th IEEE International Conference on Advanced Robotics, Monterey, CA, pp. 253–258.
[14] G. Reyne, Electromagnetic actuation for MOEMS, examples, advantages and drawbacks of MAGMAS, J. Magnet. Magnet. Mater. 242 (2002) 1119–1125.
[15] M. DeVolder, Pneumatic and hydraulic microactuators: a review, J. Micromech. Microeng. 20 (043001) (2010) 18pp.
[16] S. Bütefisch, V. Seidemann, S. Büttgenbach, Novel micro-pneumatic actuator for MEMS, Sens. Actuators A: Phys. 97 (2002) 638–645.
[17] A.J. Moers, M.F. De Volder, D. Reynaerts, Integrated high pressure microhydraulic actuation and control for surgical instruments, Biomed. Microdev. 14 (4) (2012) 699–708.
[18] K. Takemura, S. Yokota, K. Edamura, Development and control of a micro artificial muscle cell using electro-conjugate fluid, Sens. Actuators A: Phys. 133 (2) (2007) 493–499.
[19] K. Shimizu, A. Shunori, K. Morimoto, M. Hashida, S. Konishi, Development of a biochip with serially connected pneumatic balloons for cell-stretching culture, Sens. Actuators B: Chem. 156 (1) (2011) 486–493.
[20] H.W. Kang, I.H. Lee, D.W. Cho, Development of a micro-bellows actuator using micro- stereolithography technology, Microelectron. Eng. 83 (4) (2006) 1201–1204.
[21] A. Alogla, et al., A scalable syringe-actuated microgripper for biological manipulation, Sens. Actuators A: Phys. 202 (2013) 135–139.
[22] M. Kersaudy Kerhoas, F. Amalou, A. Che, J. Kelly, Y. Liu, M.P.Y. Desmulliez, W. Shu, Validation of a fully integrated platform and disposable microfluidic chips enabling parallel purification of genome segments for assembly, Biotechnol. Bioeng. 111 (8) (2014) 1627–1637.
[23] M. Milad, et al., The effect of cold work on structure and properties of AISI 304 stainless steel, J. Mater. Process. Technol. 203 (1) (2008) 80–85.
[24] W. Shu, E.D. Laue, A.A. Seshia, Investigation of biotin–streptavidin binding interactions using microcantilever sensors, Biosens. Bioelectron. 22 (2007) 2003–2009.
[25] A.N. Mehesz, J. Brown, Z. Hajdu, W. Beaver, J.V.L. da Silva, R.P. Visconti, V. Mironov, Scalable robotic biofabrication of tissue spheroids, Biofabrication 3 (2) (2011) 025002.
[26] A. Faulkner-Jones, S. Greenhough, J.A. King, J. Gardner, A. Courtney, W. Shu, Development of a valve-based cell printer for the formation of human embryonic stem cell spheroid aggregates, Biofabrication 5 (1) (2013) 015013.

Biographies

Ageel Alogla received his B.Eng. in Mechanical Engineering from the King Fahad University of Petroleum and Minerals, Kingdom of Saudi Arabia in 2002, and a Ph.D. degree from the university of Heriot-Watt on 2014. He is currently an Assistant Professor in the School of Engineering at Taif University, Kingdom of Saudi Arabia. His research interests are focused on microsystems and mechanical grippers.

Farid Amalou received his Ph.D. in MicroEngineering and MicroMagnetism at the Swiss Federal Institute of Technology in Lausanne (EPFL) in 2003. Following his postdoctoral positions at Heriot-Watt University and Southampton University, he is currently an Assistant Professor in Physics at Alfaisal University, Kingdom of Saudi Arabia.

Chris Balmer graduated with an M.Eng. degree in Mechanical Engineering from Heriot-Watt University, Edinburgh in 2014. He is currently working on his Ph.D. on the use of pneumatically actuated microgrippers for tissue quality assessment. His

research interests are focused on microgrippers and tactile feedback for biological tissues.

Paul Scanlan graduated with a B.Eng. degree in Robotics and Cybertronics from Heriot Watt University, Edinburgh in 2011. He is currently studying for his Ph.D. in the Mechanical Probing of Human Tissue. His research interests include microfabrication techniques and engineering for biomedical applications.

Wenmiao Shu received his B.Eng. degree in Polymer Materials from the Dalian University of Technology, China, in 1998, and a Ph.D. degree from the University of Cambridge in 2006. He is currently Reader of Microengineering in the School of Engineering and Physical Sciences at Heriot-Watt University. His research interests cover a range of biomedical microengineering topics including micromechanical sensors and actuators, biosensors, lab-on-a-chip systems and 3D biofabrication.

Robert L. Reuben is a Professor of Materials Engineering in the School of Engineering and Physical Sciences at Heriot-Watt University. He graduated with a First Class Honours in Metallurgy from the University of Strathclyde in 1974, after which he worked with the United Kingdom Atomic Energy Authority. In 1977 he joined the Open University's Oxford Research Unit researching the permeation characteristics to hydrogen and its isotopes of candidate fusion reactor containment materials, gaining a Ph.D. in that area in 1980. His research field includes experimental mechanics and microsystems engineering (often for medical applications), and sensor-based monitoring of machinery.